

3. THE RELATIONSHIP BETWEEN SILICA DIAGENESIS, METHANE, AND SEISMIC REFLECTIONS ON THE SOUTH ORKNEY MICROCONTINENT¹

Malcolm J. Lonsdale²

ABSTRACT

Seismic data acquired over the eastern shelf and margin of the South Orkney microcontinent, Antarctica, have shown a high-amplitude reflection lying at a sub-bottom two-way traveltime (TWT) of 0.5–0.8 s. There appear to be two causes for the reflection which apply in different parts of the shelf. The more widespread cause of the reflection is a break-up unconformity associated with the opening of Jane Basin to the east. This is clearly seen where reflections in the underlying sequence are discordant. In contrast, in Eotvos Basin and the southeastern part of Bouguer Basin, the high-amplitude reflection in places cuts across bedding and is interpreted to be caused by silica diagenesis. A post-cruise analysis of core samples from Site 696 in Eotvos Basin by X-ray diffraction (XRD) and scanning electron microscopy (SEM) revealed the presence of a silica diagenetic front at 520–530 mbsf. The position of the unconformity at this site is uncertain, but probably coincides with a change of detrital input near 548 mbsf. Fluctuations of physical properties related to the depth of the diagenetic front are difficult to separate from those related to the variation of detrital composition over the same depth interval. Correlation of the drilling record with the seismic record is difficult but with a synthetic seismogram it is demonstrated that diagenesis is the probable cause of the high-amplitude reflection.

In Bouguer Basin at Site 695 the depth of the high-amplitude reflection was not reached by drilling; however, the reflection is probably also caused by silica diagenesis because of the biogenic silica-rich composition of the sediments cored. The estimated temperatures and ages of the sediments at the depths of the high-amplitude reflections at Sites 695 and 696 compare favorably with similar data from other diagenetic fronts of the world. The high-amplitude reflection in Bouguer Basin is commonly of inverse polarity, possibly caused either by interference between reflections from several closely-spaced reflecting layers, such as chert horizons, or by free gas trapped near the diagenetic front.

INTRODUCTION

King and Barker (1988) have studied the southeastern continental shelf and margin of the South Orkney microcontinent (Fig. 1) using single-channel seismic reflection profiles and gravity and magnetic data. The profiles display two seismic sequences, S1 and S2, the lower (S2) sometimes absent, overlying acoustic basement. The boundary between S1 and S2 is a high-amplitude reflection. At several places along the profiles, reflections at the top of S2 terminate against the high-amplitude reflection, hence the causative reflector was interpreted as an unconformity. This unconformity was considered to be associated with an episode of break-up and rifting before the opening of Jane Basin (Fig. 1) which Lawver et al. (1985) consider took place in the late Oligocene, 25–30 Ma ago.

Two sedimentary basins, named after Bouguer and Eotvos by King and Barker (1988), were distinguished on the eastern continental shelf and margin (Fig. 1) using the seismic and gravity data. The basins coincide with gravity lows. Basement was not seen on the profiles near the basin axes but the horizontal extent of the basins was mapped with reference to the prominent basement highs which enclose and separate them. ODP Site 695 lies in the southeastern part of Bouguer Basin, and Site 696 lies on the southwestern margin of Eotvos Basin. Sequence S2, more than 2.0 s TWT thick in Bouguer Basin and 1.5 s TWT thick in Eotvos Basin, thins to 0.1–0.2 s TWT over the intervening basement high. Sequence S1 is of almost constant thickness at 0.5 to 0.8 s TWT in the basins and over the high.

Three multichannel seismic reflection profiles were acquired in 1985 over the southeastern continental shelf and margin, as a

site survey for ODP Leg 113. These profiles show a break-up unconformity over most of the continental shelf. However in some regions, notably in Bouguer Basin, the high-amplitude reflection is anomalous, in that it cuts across bedding. This had not been seen in the single-channel seismic data because of signal reverberation and a poorer signal-to-noise ratio.

Anomalous reflections at less than 1 s sub-bottom are seen in several continental shelf regions of the world. These reflections are interpreted to be either from the base of gas hydrate stability zones (e.g., Shipley et al., 1979) or from diagenetic fronts (e.g., Hein et al., 1978; Cooper et al., 1987).

This paper investigates the origin of the high-amplitude reflections observed on the southeastern South Orkney continental shelf at Sites 695 and 696.

DRILLING AT SITE 696

Site 696 (Shipboard Scientific Party, 1988a), at the southern margin of Eotvos Basin, was drilled at SP 365 of Multichannel seismic profile AMG845-18 (Fig. 1). At the site (Fig. 2), the high-amplitude reflection lies centrally within a group of prominent reflections spanning an interval of about 0.1 s, centered at 1.6 s TWT.

Along the profile, close to Site 696, reflections at the top of Sequence S2 terminate against the group of prominent reflections, indicating the presence of an unconformity (see Fig. 2, Shipboard Scientific Party, 1988a). The nonparallelism and tapering of reflections at the top of Sequence S2 implies overlap at the sequence boundary, typical of a nondepositional unconformity (Mitchum et al., 1977). From the reflection profile alone, it is not clear whether the unconformity corresponds to the high-amplitude reflection or lies at the time of the lowermost prominent reflection, because of interference between adjacent reflections within the group.

A sharp unconformity boundary is not seen in Hole 696B; instead, between 530 and 607 mbsf, a condensed neritic sequence of poorly dated terrigenous glauconitic sediments sepa-

¹ Barker, P. F., Kennett, J. P., et al., 1990. *Proc. ODP, Sci. Results*, 113: College Station, TX (Ocean Drilling Program).

² School of Earth Sciences, University of Birmingham, P.O. Box 363, Birmingham B15 2TT, United Kingdom.

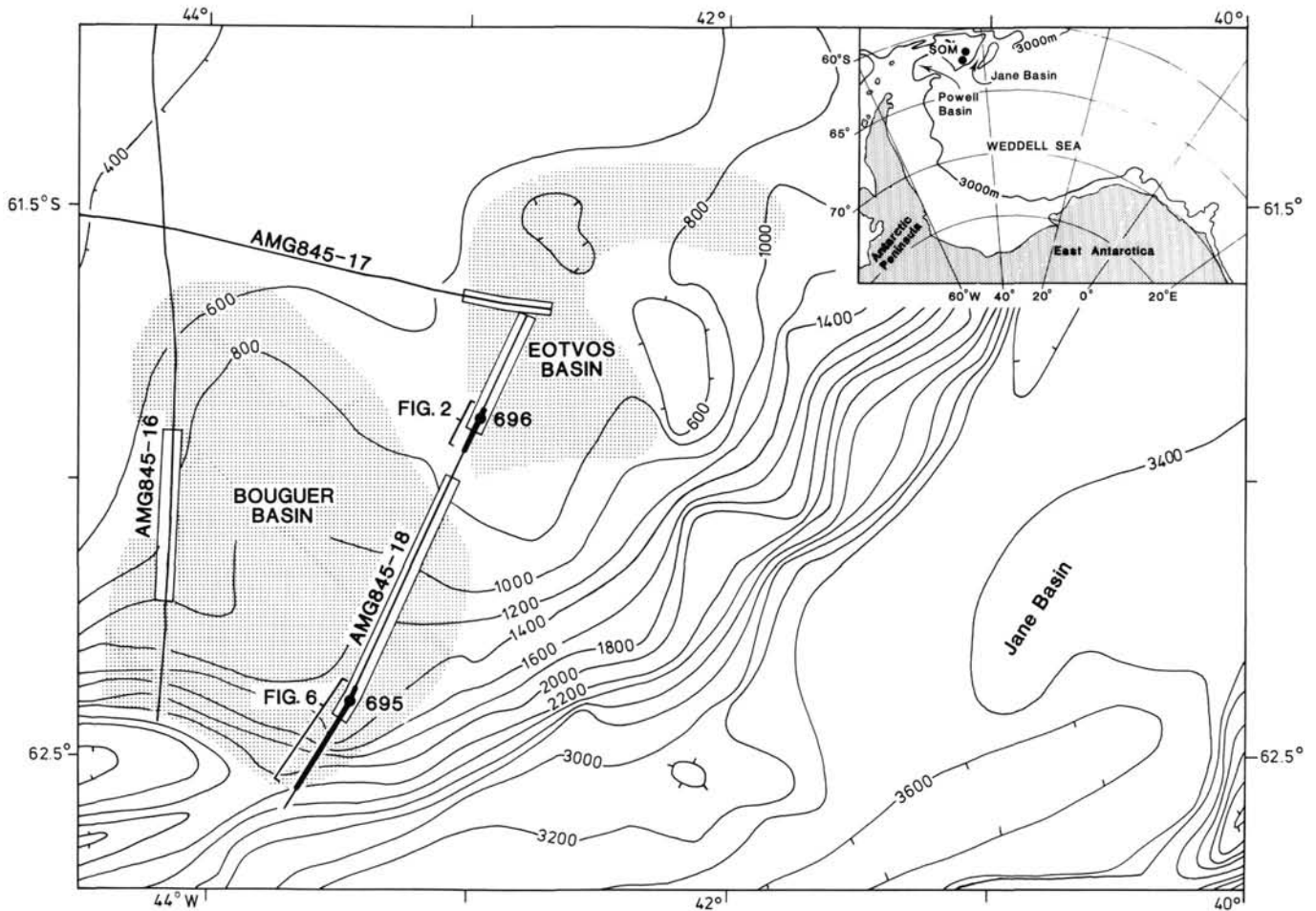


Figure 1. Bathymetric map of the southeastern continental shelf of the South Orkney microcontinent (SOM) with the locations of Multichannel seismic profiles, AMG845-16 to 18, and Sites 695 and 696. Bouguer and Eotvos Basins (stippled regions) are sedimentary basins identified by King and Barker (1988). The boxed lengths along the profiles are where the high-amplitude reflection is observed to increase in sub-bottom depth with increasing water depth. The inset map shows the regional location of the SOM; the two large dots on the SOM are the location of Sites 695 and 696.

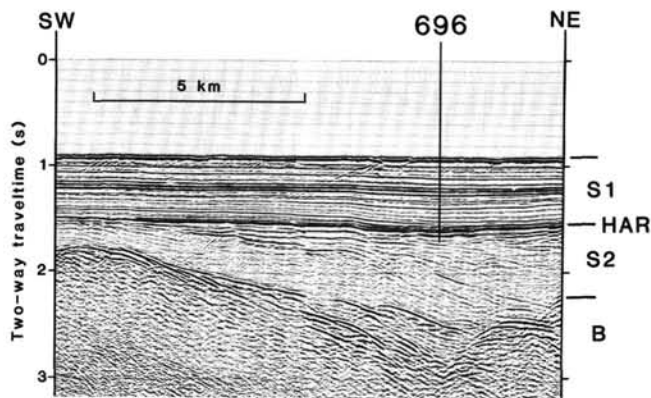


Figure 2. Twenty-four-fold seismic profile, AMG845-18, at Site 696 (location on Fig. 1). S1 and S2, Seismic sequences as defined by King and Barker (1988); HAR, high-amplitude reflection; B, acoustic basement. Note that from analysis of the drilling data, the HAR may not be from the seismic sequence boundary.

rates marine sediments of Eocene and middle Miocene age. Poor recovery and a lack of biostratigraphic control makes the exact location of any hiatus of deposition impossible; there may be an hiatus at any depth between 530 and 607 mbsf or, alternatively, sedimentation may have been slow and continuous throughout. The maximum age range of the condensed sequence, Eocene to middle Miocene, is consistent with its association with a 25–30 Ma opening of Jane Basin. It coincides with a break-up unconformity on the shelf.

At 520–530 mbsf, a major lithologic change was recorded, from muddy diatomite and mud-bearing diatomite above to sandy mudstone and claystone below (Shipboard Scientific Party, 1988a). This lithologic boundary may be either depositional or of secondary origin related to the diagenesis of biogenic silica. The boundary may contribute to the packet of prominent reflections observed at about 1.6 s TWT.

CORE SAMPLE ANALYSIS

To investigate silica diagenesis, 16 samples were taken for XRD analysis from Cores 113-696B-45R through 113-696B-54R (472.5–568.2 mbsf) (Table 1 and Fig. 3) in the vicinity of the lithologic boundary. Samples were taken at intervals of 50 cm where possible, but core recovery was poor overall.

Bulk samples were prepared for XRD analysis by grinding about 0.5 g of the dried sediment to fine powder and then

Table 1. Peak areas and heights for minerals of Hole 696B samples.

Core, section, interval (cm)	Qz	Plg	Am	Ol	A	CT	Py	Cl	Il	Ha	Co	QzO
45R-1, 97-99	12	8	—	—	255	—	—	—	12	33	—	100:11
	10	5			17			2	4	28		
46R-1, 34-36	16	32	—	—	95	—	6	—	20	15	—	100:27
	15	25			11		6	4	4	15		
47R-1, 74-76	18	24	—	13	80	—	5	—	14	18	—	100:19
	16	15		13	11		7	2	4	20		
48R-1, 61-63	9	23	—	—	210	—	5	—	15	26	—	100:10
	10	10			15		6	2	4	20		
48R-2, 98-100	10	36	2	—	195	—	4	—	14	17	—	100:18
	10	27	4		13		7	1	4	19		
49R-1, 69-71	20	22	—	—	180	—	5	4	14	22	—	100:24
	22	11			13		4	5	5	24		
50R-1, 84-86	13	33	—	—	135	—	3	—	5	16	—	100:21
	12	20			11		4	2	2	16		
50R-2, 34-36	16	167	—	—	43	—	4	2	11	13	—	100:19
	15	160			7		5	1	2	12		
51R-1, 28-30	28	109	3	—	—	170	9	4	23	3	—	100:35
	20	128	4			25	7	1	7	3		
51R-2, 49-51	18	150	—	—	—	2	2	4	10	5	—	100:31
	15	150				1	1	1	5	3		
53R-1, 19-21	111	34	7	—	—	22	5	7	12	—	11	100:23
	126	12	25			12	7	6	4		12	
53R-2, 69-71	121	40	—	—	—	3	7	8	9	—	11	100:22
	130	22				2	6	6	4		9	
53R-3, 121-123	110	35	—	—	—	6	5	6	8	—	9	100:18
	125	17				5	7	5	3		8	
53R-5, 67-69	95	13	—	—	—	210	8	8	11	—	9	100:19
	120	12				33	6	2	4		8	
54R-1, 14-16	121	20	—	—	—	11	9	7	8	—	12	100:22
	130	13				5	9	7	5		10	
54R-2, 69-71	110	37	—	—	—	165	5	8	13	—	10	100:22
	125	25				28	5	4	5		9	

Note: Units are arbitrary (i.e., chart-paper squares). Peak area and height are shown on the first and second line for each sample respectively. Qz = Quartz ($2\theta = 26.7^\circ$); Plg = Plagioclase feldspar ($27.8-28.3^\circ$); Amp = Amphibole (10.4°); Ol = Olivine (35.6°); Co = Corundum (39.6°); A = Opal-A; CT = Opal-CT (21.8°); Py = Pyrite (33.2°); Cl = Chlorite (12.5°); Il = Illite (8.9°); Ha = Halite (31.7°); —, indicates not present, QzO = ratio of first ($2\theta = 26.7^\circ$) and second (20.9°) order quartz peak heights.

spreading it evenly over a slide. Samples were run at 2θ angles of $3^\circ-40^\circ$. Approximate proportions of each mineral were calculated by taking the area of the main peak of the mineral as a proportion of the summed areas of all the main peaks of each identified mineral. No correction factors were applied; even so, semiquantitative analysis of the mineral abundances is possible. The raw peak areas and heights are given in Table 1 in order that these data may be compared with those of similar studies. Following this work, several sediment samples were photographed by SEM.

RESULTS

The minerals identified by XRD were quartz, plagioclase, amphibole, olivine, opal-A, opal-CT, pyrite, halite, and the clay minerals, chlorite, and illite. The variations in abundance of individual minerals are displayed in Figure 3. Notable downhole variations occur in quartz, plagioclase, and opal. Halite is probably a contaminant from seawater.

Five XRD patterns which summarize the major changes in mineralogy downhole are shown in Figure 4. The broad hump ($18.3^\circ-31.2^\circ$) centered on 22.1° , characteristic of opal-A (Jones and Segnit, 1971), is observed in Cores 113-696B-45R through -50R; it is of similar amplitude in Cores 113-696B-45R through -49R, but is greatly reduced in amplitude in Sample 113-696B-50R-2, 34-36 cm.

Below Core 113-696B-50R, and especially in Samples 113-696B-51R-1, 28-30 cm, 113-696B-53R-5, 67-69 cm, and 113-696B-54R-2, 69-71 cm, the opal-A reflection is replaced by reflections of varying amplitude centered at around 21.7° and 35.9° (Fig. 4). These peaks are attributed to opal-CT (Jones and

Segnit, 1971). A small "shoulder" peak, usually observed on the much larger peak at 21.7° and attributed to low tridymite (Jones and Segnit, 1971), is hidden by the secondary quartz peak which occurs at roughly the same position; however, the quartz peak is asymmetric, indicating that low tridymite may be present.

SEM photographs of diatom skeletons display the increasing fragmentation of and effect of dissolution on individual frustules with increasing depth. In Cores 113-696B-45R through 113-696B-49R, complete diatom skeletons are common (Pl. 1, Figs. 1 and 2), but below Core 113-696B-50R only sparse skeletal fragments are observed.

Lepidospheres of opal-CT crystals are found occupying the voids and overgrowing the molds of recrystallized diatom tests (Pl. 1, Figs. 3 and 4) in Samples 113-696B-51R-2, 49-51 cm, 113-696B-53R-5, 67-69 cm, and 113-696B-54R-2, 69-71 cm. Energy-dispersive X-ray analysis (EDAX) of individual lepidospheres showed that while their dominant chemical composition is silica, minor quantities of titanium, sodium, and calcium are also present. Tridymite twinning, confirming the identification of opal-CT, was recognized in the crystals of lepidospheres on several SEM photographs (Pl. 1, Fig. 3).

Hence, although isolated chert horizons occur at 357, 463, 490, and 520 mbsf (Shipboard Scientific Party, 1988a), XRD analysis indicates that a significant diagenetic front occurs between 520 and 532 mbsf. At this depth, there is a significant reduction of opal-A; this is replaced by the sporadic occurrence of opal-CT.

The variation of opal-CT abundance below 532 mbsf (Fig. 3) may be explained by migration of silica-rich pore fluids in the

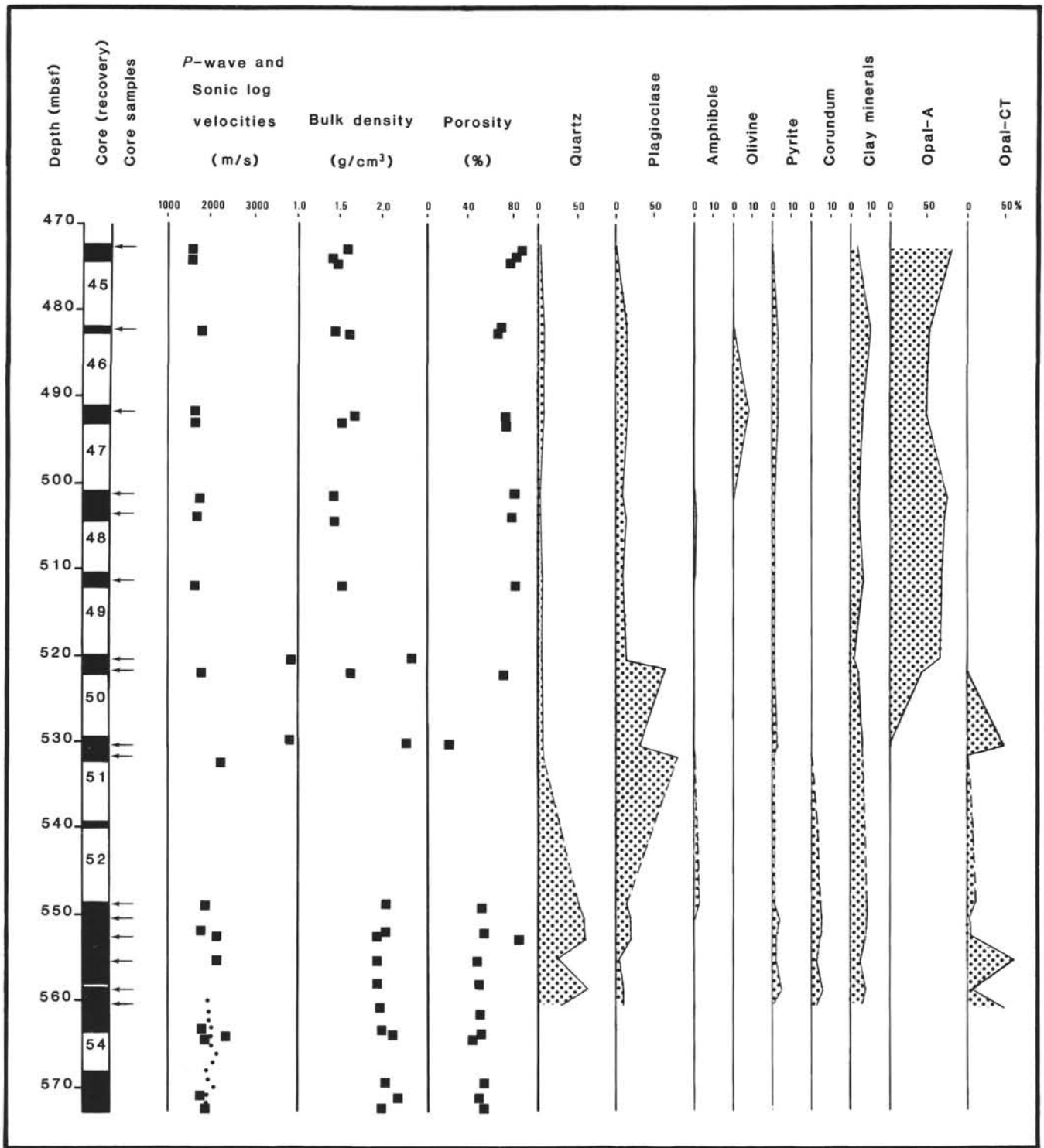


Figure 3. Site 696, core recovery, sample location, physical properties, and approximate proportions of minerals sampled for the interval where diagenetic processes are present. Sonic log data are displayed as dots together with *P*-wave velocities (Hamilton Frame) measured in the laboratory. Core numbers are positioned beneath the lengths of recovered core. (Core 53 is not shown).

sediments over ranges of centimeters to meters (e.g., Heath and Moberly, 1971). It is also possible that the lithology (variations in the quantity of quartz and plagioclase or type of clay minerals present in individual horizons) influences the rate and degree of silica diagenesis (Kastner et al., 1977).

At about 522 and 532 mbsf, plagioclase feldspar dominates the mineral suite. Quartz replaces feldspar as the dominant mineral below 549 mbsf.

The plagioclase is calcium-rich, identified in smear slides by the angles of extinction of Carlsbad-Albite twinning in individ-

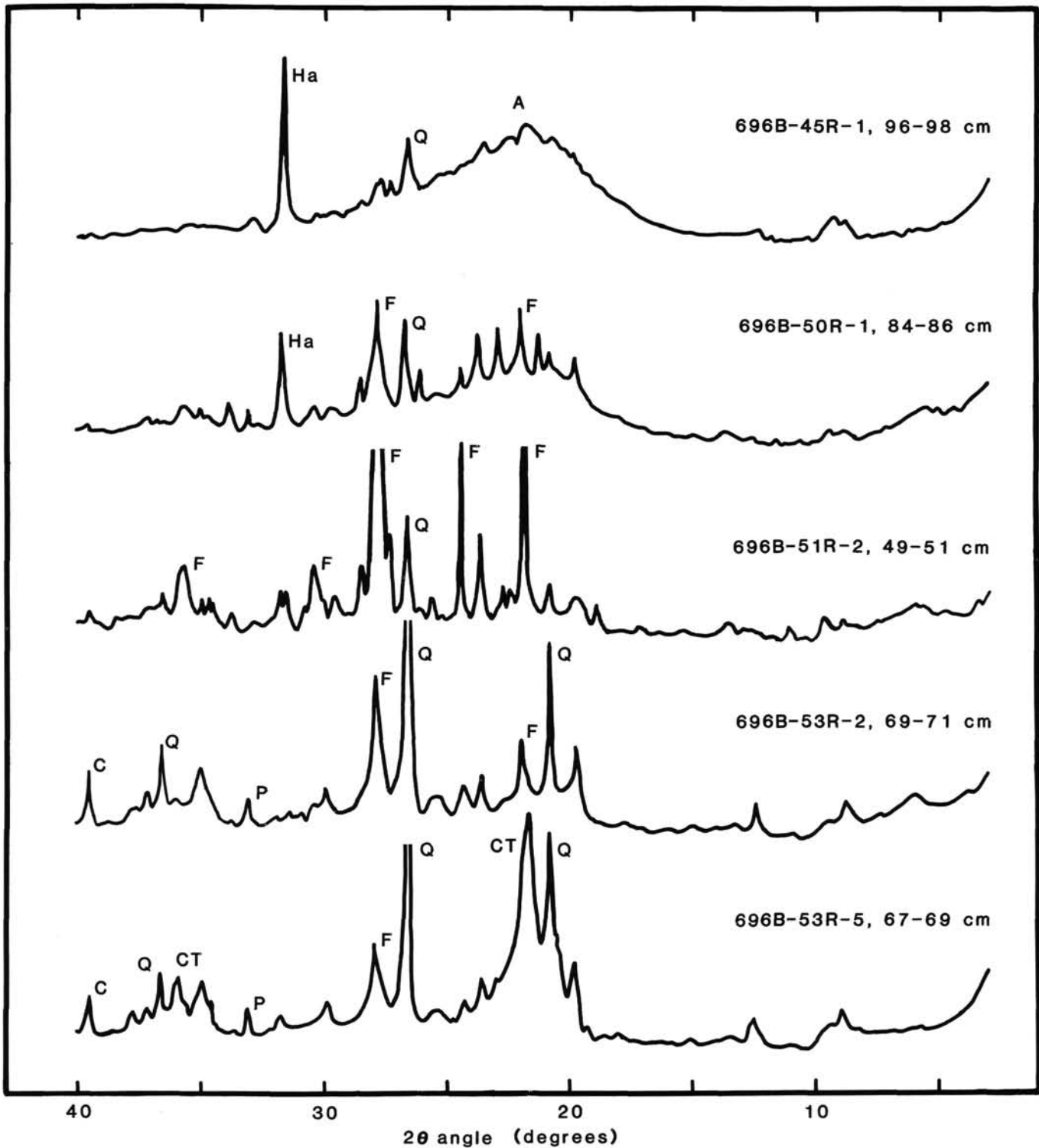


Figure 4. X-ray diffractograms of five samples displaying characteristic opal-A and opal-CT patterns. With increasing depth the opal-A mound disappears to be replaced by the narrower, taller opal-CT X-ray reflection. Great abundances of quartz and plagioclase feldspar are displayed in the intervening samples. Q = Quartz, P = Pyrite, F = Plagioclase feldspar, Ha = Halite, C = Corundum, CT = Opal-CT, A = Opal-A.

ual crystals; therefore, it is probably of detrital origin (Kastner and Siever, 1979).

The plagioclase may be volcanogenic, perhaps related to the volcanism of Jane Bank (Barker et al., 1984). The reduction in

quantity of plagioclase above Section 113-696B-50R-2 would therefore indicate the cessation of deposition of volcanogenic sediments from Jane Bank, after initial rifting and prior to the spreading in Jane Basin. Alternatively, an upward increase of

the biosiliceous sedimentation rate would reduce the proportion of plagioclase in the deposited sediments if the rate of plagioclase deposition remained constant.

The height ratio of the first and second order quartz peaks (at 26.7° and 21.9°) lies between 100:11 and 100:35 (Table 1), so the quartz is of mixed detrital and diagenetic origin (J. R. Hein, pers. comm., 1989).

Corundum is identified in samples from Cores 113-696B-53R and -54R, on the basis of four distinct peaks on the X-ray diffractogram; this mineral is of detrital origin and may have the same provenance as the quartz, since in those cores quartz is more abundant. Corundum occurs as an accessory mineral in some igneous rocks, as a common primary mineral in some igneous rocks such as nepheline-syenites, and by metamorphism of shale and limestone. Although corundum has not been reported from the South Orkney Islands (e.g., Thomson, 1974), the metamorphic rocks present on the islands are potential sources.

PHYSICAL PROPERTIES ASSOCIATED WITH DIAGENESIS

The cementation of sediments that occurs with the opal-A to opal-CT transformation causes an increase in both density and seismic velocity, producing a downward increase in acoustic impedance, such as that observed by Scholl and Creager (1973) in Bering Sea sediments of late Miocene age.

Core recovery at Site 696 was 61% down to 144 mbsf, 43% from 473 mbsf to the base of Hole 696B, but only 16% in between. Physical properties measurements are insufficient for the calculation of a complete synthetic seismogram, which therefore prevents a simple, precise correlation of the drilling record with the seismic profile.

In situ downhole physical properties were measured using borehole logging, from 605 to 550 mbsf (sonic log data in Fig. 3), before loss of the logging tool. The average velocity recorded by the sonic log was 2190 m/s; major deviations from this value were interpreted to be the result of hole diameter variation as recorded by the caliper log (Shipboard Scientific Party, 1988a).

Despite these problems, an attempt was made to correlate the seismic profile, physical properties, and lithologic record in the region of the possible unconformity. A synthetic seismogram was generated from shipboard *P*-wave velocity and saturated bulk density measurements on core samples from the lowermost section of the hole. The input wavelet (inset in Fig. 5) for the synthetic seismogram (designed from the seafloor reflection of the deconvolved and stacked multichannel seismic data) is 70 ms in length, and the first major deflection of the wavelet occurs 20 ms after the causative impedance contrast. The optimal position of the synthetic seismogram on the seismic profile (Fig. 5) was chosen on the basis of the correlation of the major reflections, although some reflections do not match well, mainly because of poor recovery between 532.3 and 548.9 mbsf.

The average velocity of the overlying sediments implied by this optimal position was 1516 m/s, which compares well with the average velocity of 1550 m/s measured on core samples aboard ship. Similar low velocities measured on the better-sampled sediments at Site 695 were attributed to their high diatom concentration (Shipboard Scientific Party, 1988b). Thus if it is assumed that the poorly sampled sediments above 470 mbsf at Site 696 are also all highly diatomaceous, then the optimal correlation of synthetic and observed seismic profiles proposed here seems reasonable.

Constructive interference between reflections from chert horizons between 520 and 530 mbsf (Shipboard Scientific Party, 1988a) is considered responsible for the high-amplitude reflection on the synthetic seismogram; the optimal correlation posi-

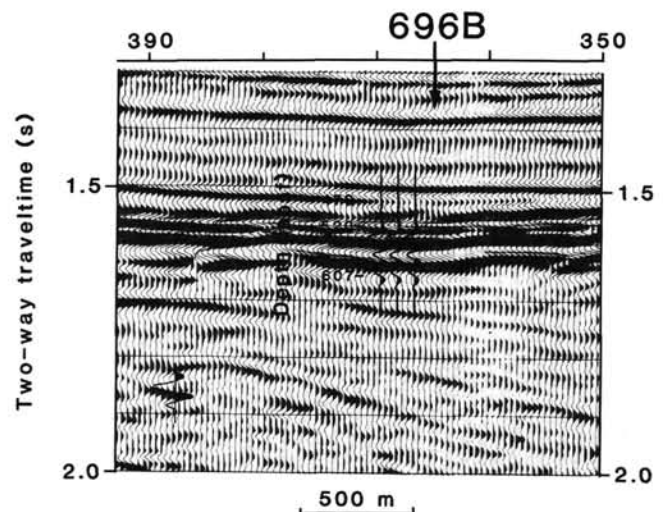


Figure 5. Optimal position of the synthetic seismogram for the lower section of Hole 696B using downhole *P*-wave velocity and density measurements. Inset, and at the same scale as the seismic section, is the input wavelet designed from the seafloor reflection.

tions this reflection at 1.60 s TWT to align with the major reflection of the prominent group of reflections on the seismic data (Fig. 5). Other prominent reflections near 1.6 s TWT on the profile are not well matched by the synthetic seismogram, an indication of the inadequate core recovery and physical properties measurement.

Measured physical properties are displayed alongside the XRD results in Figure 3. The poor core recovery at the depth of the diagenetic front (probably between 520 and 532 mbsf), and between 532.3 and 548.9 mbsf, hinders proper correlation of physical property changes with diagenesis. However, a general overview of physical properties is possible.

Between 520 and 550 mbsf, *P*-wave velocity increases from an average of around 1800 m/s to 2000 m/s, bulk density increases from 1.5 to about 1.9 g/cm³, and porosity decreases from 75% to about 44% (Shipboard Scientific Party, 1988a).

Although the influence of silica diagenesis on physical properties is apparent, it is also possible that varying quantities of detrital minerals, such as quartz, plagioclase, and corundum, will influence the properties.

Hence, the prominent reflections at about 1.6 s TWT are interpreted to be the combined interference effect of reflections from several horizons comprising diagenetically-derived opal-CT and major variations of the detrital content of the sediments.

An unconformity could be correlated with one of the alterations of detrital input, such as that at 548.9 mbsf where abundances of quartz and corundum increase downward; however, its reflection would be difficult to correlate with the seismic profile because of low recovery and interference with other reflections from near that depth.

INTERPRETATION OF SEISMIC DATA ACQUIRED OVER BOUGUER BASIN NEAR SITE 695

High-amplitude reflections are also seen on Profile AMG845-18 over the southeastern region of Bouguer Basin. Of particular interest is the relationship of the high-amplitude reflection in the vicinity of Site 695 to bedding reflections (Fig. 6). Bedding reflections above and beneath the high-amplitude reflection are generally concordant; however, the high-amplitude

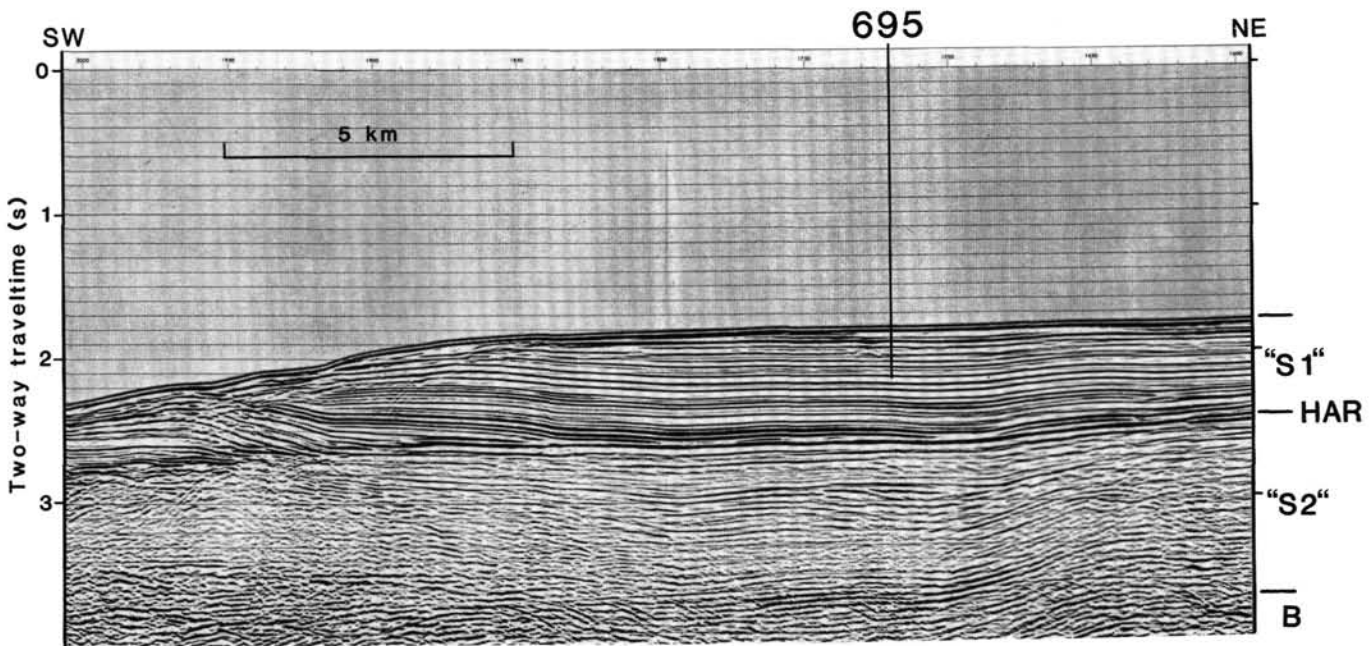


Figure 6. Twenty-four-fold seismic profile, AMG845-18, at Site 695 (location on Fig. 1). Note that if the HAR is of secondary origin, the boundary between Sequences S1 and S2 is not located. Hence, the names S1 and S2 are placed in quotes to signify the incomplete seismic stratigraphic interpretation of this section.

reflection is variably discordant to this bedding and especially, between SP 1625 and SP 1700 at 2.4–2.6 s TWT, and SP 1800 and 1950, at 2.6–2.7 s TWT. Such reflection geometry is evidence for secondary geologic processes and not for an unconformity boundary as the cause for the high-amplitude reflection.

It is possible to trace the high-amplitude reflection and overlying reflections at Site 695 along the profile to Site 696. Only the uppermost 370 ms of the section at Site 696 lies above the high-amplitude reflection at Site 695. Deeper reflections at Site 696 appear to cross the high-amplitude reflection on the way to Site 695 and, since the high-amplitude reflection is probably caused by secondary processes, probably lie beneath it at the site. The regional break-up unconformity correlated at Site 696 with the poorly-dated terrigenous sediments below 530 mbsf cannot be clearly seen near Site 695. It should lie well below the high-amplitude reflection, but is difficult to identify because of the lower amplitude of all reflections beneath the high-amplitude reflection.

It was postulated, prior to drilling, that the high-amplitude reflection was either from a diagenetic front or from the base of a gas hydrate stability zone.

Results at Site 695

Site 695 (Shipboard Scientific Party, 1988b) is situated in the southeastern region of Bouguer Basin at SP 1720 of Profile AMG845-18 (Fig. 6).

Drilling at Hole 695A penetrated to 341.1 mbsf, where shearing of the XCB corer in the hole prevented drilling to the depth of the major reflector, estimated to lie at about 690 mbsf.

The sediments sampled at Site 695 are rich in biogenic silica, and correlate straightforwardly along Profile AMG845-18 with the upper part of the drilled section at Site 696. The continued high silica content of the deeper sediments at Site 696 suggests that the deeper, undrilled part of the section above the major reflector at Site 695 is also highly siliceous. It is therefore reasonable that the major reflector at Site 695 should result from silica diagenesis.

Hein et al. (1978) reviewed the temperature-age relationship for the transformation of opal-A to opal-CT in moderately to highly siliceous sediments worldwide. Similar temperature-age data may be calculated for the high-amplitude reflection at Sites 695 and 696 (Table 2). The temperature at Site 696 may be calculated approximately from the rather sparse thermal conductivity measurements and temperatures measured higher in the section at this site. Similar, more numerous thermal conductivity and temperature measurements in the drilled section can be extrapolated to the depth of the major reflector at Site 695, and the age there can be estimated by correlation with Site 696 along Profile AMG845-18. Temperature-age data so estimated are consistent with the Hein et al. (1978) dataset (Fig. 7), supporting the interpretation of silica diagenesis as the cause of the high-amplitude reflection at Site 695.

Evidence for the Formation of Gas Hydrate

An alternative explanation offered for the high-amplitude reflection before drilling was the formation of gas hydrate. Two features observable on a seismic profile are normally used to indicate the presence of gas hydrate: the reflection which correlates with the base of the gas hydrate layer will simulate the seafloor reflection and be of inverse polarity (Shiple et al., 1979).

Sub-bottom Depth of the High-amplitude Reflection

In oceanic sediments, the conditions of pressure and temperature at which gas hydrate is stable are such that the base of the

Table 2. Estimated age and temperature data at the depths of the diagenetic fronts at Sites 695 and 696.

	Site 695	Site 696
Depth (mbsf)	690?	520–530
Temperature (°C)	40.5 ± 2?	32 ± 2?
Sediment age (Ma)	11?	15

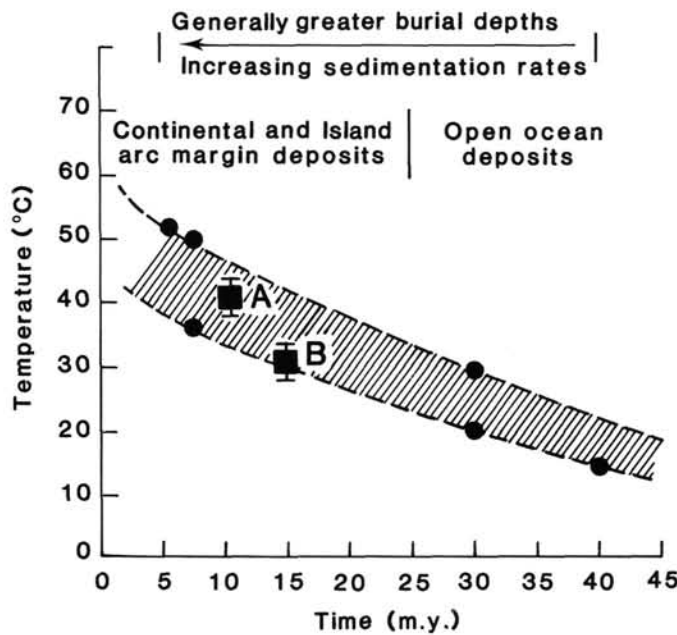


Figure 7. Estimated time and temperature field necessary for initiation of the opal-A to opal-CT transformation for highly to moderately siliceous deep sea deposits (after Hein et al., 1978). A and B are the plots of Sites 695 and 696, respectively, from Table 2.

gas hydrate stability zone will commonly increase in sub-bottom depth with increasing water depths, assuming a regionally-uniform geothermal gradient. In Figure 8, the TWT to the seafloor is plotted against the sub-bottom TWT to the high-amplitude reflection for Eotvos and Bouguer Basins along Profile AMG845-18. In both basins, the high-amplitude reflection increases in sub-bottom depth as water depth increases, consistent with gas hydrate formation in these regions. The different slopes from the two basins would imply a change of geothermal gradient between the basins. The lengths of multichannel profile where this relationship is observed are shown in Figure 1.

Apparent Polarity of the High-amplitude Reflection

Stoll et al. (1971) demonstrated that gas hydrate increases the rigidity and seismic velocity of the host sediment. Therefore, at the base of a stability zone containing gas hydrate, a velocity inversion is expected. This will be enhanced if free gas is also trapped against the base of the stability zone which may have a low permeability and act as a cap rock.

To study the polarity of the high-amplitude reflection, complex seismic trace attribute analysis (Taner et al., 1979) was used. The apparent polarity of the high-amplitude reflection was calculated for SP 1550-2050, in the region of Site 695. Over most of this length, the reflection was found to be of inverse polarity, consistent with its origin from the base of a gas hydrate stability zone. (The inverse polarity of this reflection was observed at all stages of seismic data processing, so it is not an artifact of processing.) The inverse polarity of the high-amplitude reflection is illustrated in Figure 9 by five apparent polarity traces calculated by trace attribute analysis from the processed seismic data at Site 695. Similar examination of the high-amplitude reflection in Eotvos Basin near Site 696 showed it to be of normal polarity.

Hence, analysis of the seismic profiles over Bouguer Basin would suggest the presence of gas hydrate. Further analysis of the high-amplitude reflection in Bouguer Basin is possible with temperature and thermal conductivity data acquired at Site 695.

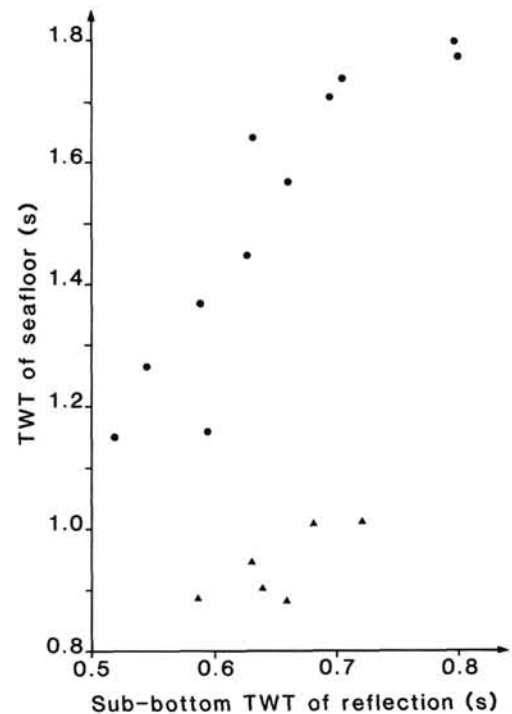


Figure 8. Two-way traveltimes to seafloor vs. sub-bottom two-way travel-time of the high-amplitude reflection along Profile AMG845-18. Data were picked at 100 SP intervals. Triangles are for SP 1-500 in Eotvos Basin and dots are for SP 800-1800 in Bouguer Basin.

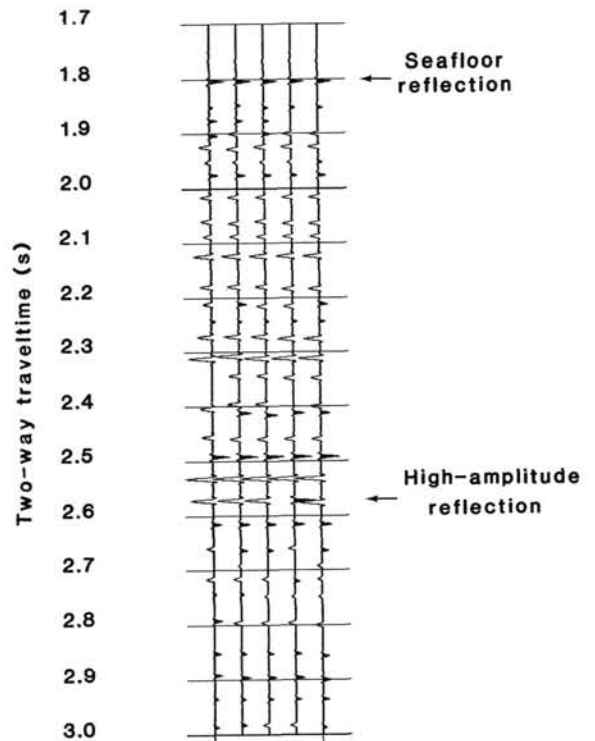


Figure 9. Five apparent polarity traces calculated by trace attribute analysis from stacked multichannel seismic data at Site 695. A deflection of the trace to the right indicates normal polarity and a deflection to the left indicates inverse polarity. Note the reversed polarity of the high-amplitude reflection and the numerous reversed polarity reflections in the overlying sequence.

Heat Flow Studies

From temperature and thermal conductivity measurements made during drilling, a heat flow of $65 \pm 5\%$ mW/m² and an average geothermal gradient of $52^\circ \pm 2^\circ\text{C}/\text{km}$ were calculated.

As gas hydrate stability is strongly dependent upon temperature, it is possible to calculate the local heat flow and temperature gradient from the depth of a postulated hydrate bottom-simulating reflection. Using MacLeod's (1982) hydrate stability curves for pure methane hydrated in Arctic seawater, it is estimated that if the high-amplitude reflection at Site 695 is from the base of a gas hydrate stability zone, then the geothermal gradient would be $24^\circ \pm 2^\circ\text{C}/\text{km}$. This value is half the geothermal gradient measured at the site, so gas hydrate would not be stable at the depth of the high-amplitude reflection.

Thus, despite the seismic evidence for the presence of gas hydrate, heat flow data show conclusively that hydrate cannot cause the high-amplitude reflection in Bouguer Basin. Therefore, it is stressed that caution is necessary when inferring the presence of gas hydrate from seismic data alone.

The Inverse Polarity of the High-amplitude Reflection in Bouguer Basin

Diagenetically-altered sediments have a higher *P*-wave velocity, so the inverse polarity of the high-amplitude reflection in Bouguer Basin is not explained by a simple diagenetic boundary. It is possible that the high-amplitude reflection originates from a zone of thin, closely-spaced alternating high/low velocity layers, such as chert horizons, at the diagenetic front. Complex diagenetic fronts have been drilled in areas such as the outer edge of the Beringian Shelf (Turner et al., 1984). The inverse polarity could result from interference between reflections from horizons at a complex diagenetic front.

Evidence to support this interpretation is found in Eotvos Basin where the polarity of the high-amplitude reflection is predominantly normal. Between SP 361 and 382 (Fig. 5), around Site 696, a reflection at a sub-bottom TWT of 1.61 s (approximately 520 mbsf) is of inverse polarity. This localized polarity inversion may be caused by interference between reflections from the upper and lower boundaries of chert horizons, three of which were sampled between 460 and 540 mbsf. That the polarity of the high-amplitude reflection changes to become dominantly normal elsewhere in Eotvos Basin may indicate variation of the number and spacing of chert horizons. A similar situation in Bouguer Basin may explain the mainly inverse polarity of the high-amplitude reflection.

Levels of light hydrocarbons were low at Site 696 above 611 mbsf. Nevertheless, the amplitude of any reflection from a suite of chert horizons, in Bouguer or Eotvos basins, would be increased if free gas were trapped beneath one or more cherts, increasing acoustic impedance contrasts.

Evidence for Methane Hydrate in Bouguer Basin

At Site 695, concentrations of methane increase logarithmically below 259 mbsf; this occurs at a depth where the sulfate concentration in interstitial waters has reduced close to zero, a necessary precursor to methanogenic activity (Claypool and Kaplan, 1974), so the methane is interpreted to be of biogenic origin.

With a local heat flow of 65 mW/m² and assuming a pure methane composition, it was calculated that the approximate depth of the base of a hydrate stability zone would be 335 ± 20 mbsf. This depth corresponds to 2.20 ± 0.02 s TWT by using interval velocity data from a nearby VELAN at SP 1741. Although moderate-amplitude inverse polarity reflections occur at 2.18 and 2.22 s TWT (Fig. 9), they do not cross bedding planes, nor increase in depth sub-bottom as the seafloor depth increases (Fig. 6).

Thus, although methane was recovered at the site at the depth at which methane hydrate is stable, there is no seismic evidence for widespread hydrate formation at this locality.

CONCLUSIONS

1. Previous seismic data interpretation had correlated a high-amplitude reflection with a regional break-up unconformity. At Site 696, although identified on seismic data, an erosional unconformity was not confirmed by drilling because of poor recovery and the lack of biostratigraphic data. A change in the detrital component near 548 mbsf may indicate the position of an unconformity. However, a silica diagenetic boundary at 520–530 mbsf is interpreted as the probable cause of the high-amplitude reflection. In Bouguer Basin, near Site 695, silica diagenesis is interpreted as the cause of a high-amplitude reflection. Any break-up unconformity will lie deeper in Bouguer Basin and its impedance contrast may be suppressed by diagenesis.

2. At Site 696, variations of physical properties associated solely with silica diagenesis were difficult to isolate, because there are fluctuations of detrital composition over the same depth interval, and core recovery was low. However, observed variations in density and velocity, regardless of cause, were sufficiently large to explain the high-amplitude reflection.

3. Despite strong seismic evidence for the high-amplitude reflection to be correlated with gas hydrate formation in Bouguer Basin, this interpretation is ruled out on the evidence of temperature and thermal conductivity data acquired at Site 695. Extreme caution is urged when interpreting the presence of gas hydrate on the evidence of seismic data alone; neither inverse polarity nor correlation with hydrate stability behavior is diagnostic.

4. The cause of the inverse polarity of large proportions of the high-amplitude reflection in Bouguer Basin remains anomalous. It is possible that it originates from interference between reflections from several closely-spaced reflectors, such as chert horizons, or is caused by free gas trapped in the vicinity of the diagenetic boundary.

5. No strong anomalous reflection is observed at Site 695 at the depth at which the base of a methane hydrate layer would be stable, although methane was detected in logarithmically increasing quantities near the base of Hole 695A.

ACKNOWLEDGMENTS

I would like to thank Dr. Peter Barker for his helpful guidance and comments concerning this research. The help of Drs. Carol Pudsey and Ian Fairchild in advising and helping me to prepare, analyze, and interpret the core samples and data was much appreciated. I would also like to thank the officers and crew of *Discovery* and the technicians from Research Vessel Services, Barry, South Wales for their expertise and assistance in acquiring the multichannel seismic data over the South Orkney microcontinent on Cruise 154, in 1985.

My appreciation goes to Drs. P. F. Barker, A. K. Cooper, J. R. Hein, C. M. Isaacs, S. O'Connell, and C. J. Pudsey who read and made constructive comments to improve the original manuscript.

REFERENCES

- Barker, P. F., Barber, P. L., and King, E. C., 1984. An early Miocene ridge crest-trench collision on the South Scotia Ridge near 36°W . *Tectonophysics*, 102:315–332.
- Claypool, G. E., and Kaplan, I. R., 1974. The origin and distribution of methane in marine sediments. In Kaplan, I. R. (Ed.), *Natural gases in marine sediments*: New York (Plenum), 99–139.
- Cooper, A. K., Scholl, D. W., and Marlow, M. S., 1987. Structural framework, sedimentary sequences and hydrocarbon potential of the Aleutian and Bowers Basins, Bering Sea. In Scholl, D. W., Grantz, A., and Vedder, J. G. (Eds.), *Geology and resource potential of the continental margin of western North America and adjacent*

- ocean basins—Beaufort Sea to Baja California*. Circum-Pacific Council for Energy and Mineral Resources, Houston, 6:473–502.
- Florke, O. W., Hollman, R., von Rad, U., and Rosch, H., 1976. Inter-growth and twinning in opal-CT lepispheres. *Contrib. Mineral. Petrol.*, 58:235–242.
- Heath, G. R., and Moberly, R., 1971. Cherts from the Western Pacific, Leg 7, Deep Sea Drilling Project. In Winterer, E. L., et al., *Init. Repts. DSDP, 7*: Washington (U.S. Govt. Printing Office), 991–1007.
- Hein, J. R., Scholl, D. W., Barron, J. A., Jones, M. G., and Miller, J., 1978. Diagenesis of late Cenozoic diatomaceous deposits and formation of the bottom-simulating reflector in the southern Bering Sea. *Sedimentology*, 25:155–181.
- Jones, J. B., and Segnit, E. R., 1971. The nature of opal. 1. Nomenclature and constituent phases. *J. Geol. Soc. Aust.*, 18:57–68.
- Kastner, M., Keene, J. B., and Gieskes, J. M., 1977. Diagenesis of siliceous oozes 1. Chemical controls on the rate of opal-A to opal-CT transformation—an experimental study. *Geochim. Cosmochim. Acta*, 41:1041–1059.
- Kastner, M., and Siever, R., 1979. Low temperature feldspars in sedimentary rocks. *Am. J. Sci.*, 279:435–479.
- King, E. C., and Barker, P. F., 1988. The margins of the South Orkney microcontinent. *J. Geol. Soc. (Lond.)*, 145:317–331.
- Lawver, L. A., Della Vedova, B., and Von Herzen, R. P., 1985. Heatflow measurements in the Jane Basin, a back-arc basin, northern Weddell Sea. *Antarct. J. U.S.*, 19(5):87–88.
- MacLeod, M. K., 1982. Gas hydrates in ocean bottom sediments. *Am. Assoc. Pet. Geol. Bull.*, 66:2649–2662.
- Mitchum, R. M., Vail, P. R., and Thompson, S., 1977. Seismic stratigraphy and global changes of sea level, Part 2: The depositional sequence as a basic unit for stratigraphic analysis. In Payton, C. E. (Ed.), *Seismic stratigraphy—applications to hydrocarbon exploration*: Am. Assoc. Pet. Geol. Mem., 26:53–62.
- Scholl, D. W., and Creager, J. S., 1973. Geological Synthesis of Leg 19 (DSDP) results; far north Pacific, and Aleutian Ridge and Bering Sea. In Creager, J. S., Scholl, D. W. et al., *Init. Repts. DSDP, 19*: Washington (U.S. Govt. Printing Office), 897–913.
- Shipboard Scientific Party, 1988a. Site 696. In Barker, P. F., Kennett, J. P., et al., *Proc. ODP, Init. Repts.*, 113: College Station, TX (Ocean Drilling Program).
- , 1988b. Site 695. In Barker, P. F., Kennett, J. P., et al., *Proc. ODP, Init. Repts.*, 113: College Station, TX (Ocean Drilling Program).
- Shipley, T. H., Houston, M. H., Buffler, R. T., Shaub, F. J., McMillen, K. J., Ladd, J. W., and Worzel, J. L., 1979. Seismic evidence for widespread possible gas hydrate horizons on continental slopes and rises. *Am. Assoc. Pet. Geol. Bull.*, 63:2204–2213.
- Stoll, R. D., Ewing, J., and Bryan, G. M., 1971. Anomalous wave velocities in sediments containing gas hydrates. *J. Geophys. Res.*, 76:2090–2094.
- Taner, M. T., Koehler, F., and Sheriff, R. E., 1979. Complex seismic trace analysis. *Geophysics.*, 44:1041–1063.
- Thomson, J. W., 1974. The geology of the South Orkney Islands: III. Coronation Island. *Br. Antarct. Surv. Sci. Repts.*, 86.
- Turner, R. F., McCarthy, C. M., Steffy, D. A., Lynch, M. B., Martin, G. C., Sherwood, K. W., Flett, T. O., and Adams, A. J., 1984. Geological and operational summary, Navarin Basin COST No. 1 well, Bering Sea, Alaska. *Min. Manag. Serv. OCS Rept.* MMS 84–0031.

Date of initial receipt: 27 September 1988

Date of acceptance: 8 August 1989

Ms 113B-177

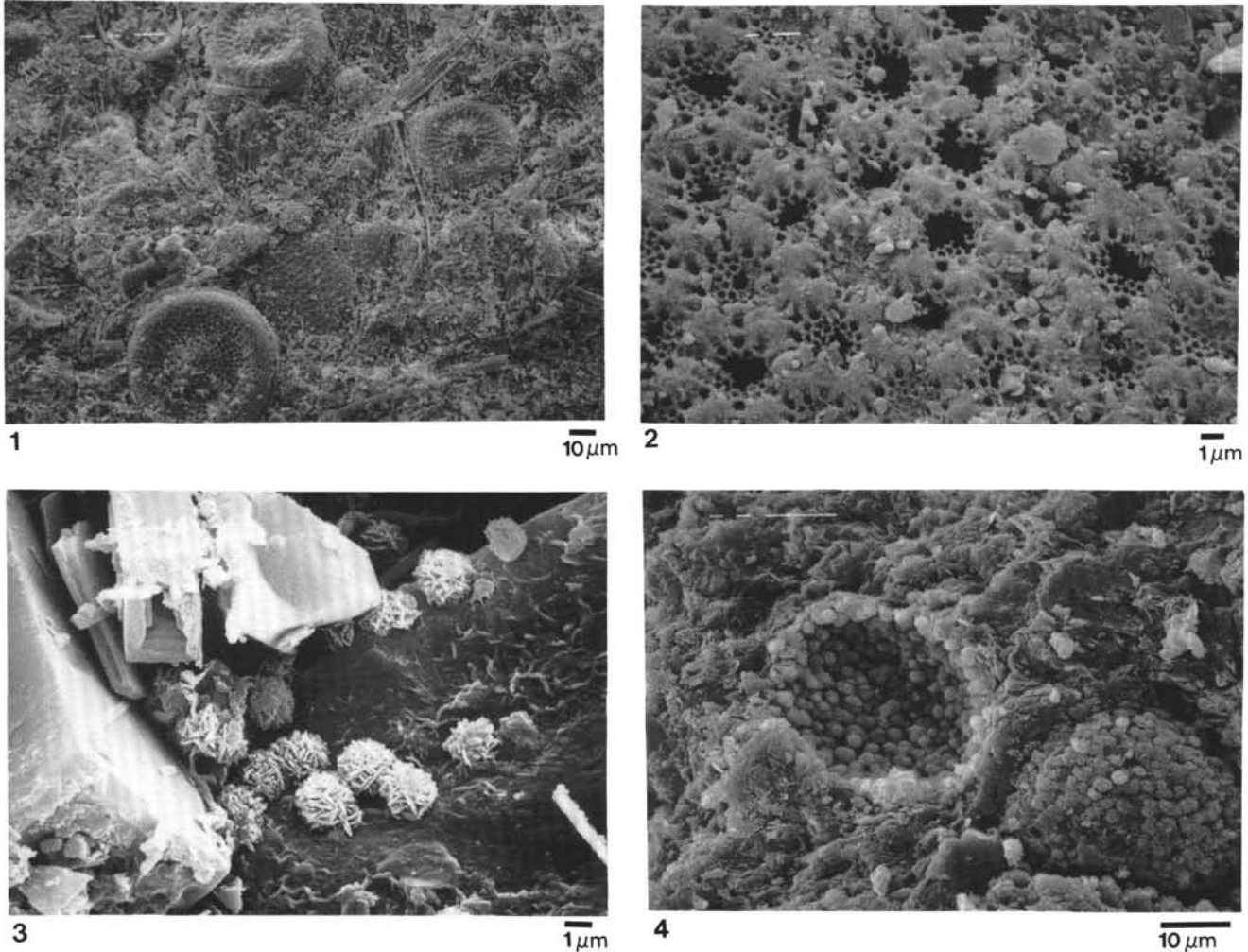


Plate 1. Scanning electron micrographs of opal-A and opal-CT. **1.** Mud-bearing diatomite with well preserved opaline (opal-A) skeletons and fragments of diatoms. Sample 113-696B-45R-1, 96-98 cm (Subunit VIB, middle Miocene). **2.** Partially dissolved diatom skeleton. The finer branches of the test are more quickly dissolved than the nodes. Sample 113-696B-50R-2, 34-36 cm (Subunit VIB, middle Miocene). **3.** Detail of bladed opal-CT lepispheres with regular 70° or 180°-70° angles recording the twinning law of tridymite (Florke et al., 1976). Sample 113-696B-51R-2, 49-51 cm (Subunit VIIA, middle Miocene). **4.** Clusters of opal-CT lepispheres attached to the walls of a cavity and mound. Sample 113-696B-53R-5, 67-69 cm (Subunit VIIB, early Miocene to late Paleogene).